Bulletin of the Seismological Society of America, Vol. 92, No. 2, pp. 641–655, March 2002

Aftershock Zone Scaling

by Yan Y. Kagan

Abstract We investigate the distribution of aftershock zones for large earthquakes (scalar seismic moment $M \geq 10^{19.5}$ N m, moment magnitude, $m \geq 7$). Mainshocks are selected from the Harvard centroid moment tensor catalog, and aftershocks are selected from the Preliminary Determination of Epicenters (NEIC) catalog. The aftershock epicenter maps are approximated by a two-dimensional Gaussian distribution; the major ellipse axis is taken as a quantitative measure of the mainshock focal zone size. The dependence of zone length, l, on earthquake size is studied for three representative focal mechanisms: thrust, normal, and strike slip. Although the numbers of mainshocks available for analysis are limited (maximum a few tens of events in each case), all earthquakes show the same scaling ($M \propto l^3$). No observable scaling break or saturation occurs for the largest earthquakes ($M \geq 10^{21}$ N m, $m \geq 8$). Therefore, it seems that earthquake geometrical focal zone parameters are self-similar.

Introduction

Earthquake rupture is characterized by three geometric quantities: length of the rupture, l, width, W, and average slip, u. Seismic moment, M, is defined through these quantities as

$$M = \mu u W l, \tag{1}$$

where μ is the elastic shear modulus.

The scaling relations between M and the geometrical parameters in (1) have attracted seismologists' attention for many years. Kanamori and Anderson (1975), Geller (1976), and Sato (1979) proposed that for small and moderate earthquakes the scalar moment M is proportional to the cube of its focal length l

$$M \propto l^d, \tag{2}$$

with $d = 3$. However, they suggested that for larger earthquakes, this scaling relation breaks down, with $d = 2$ for large earthquakes or even $d = 1$ for the largest ones.

The reason for postulating such a breakdown is usually formulated as follows. For small earthquakes the rupture propagates entirely within the brittle crust, whereas for large earthquakes rupture is confined to the upper crust layer of thickness W. Thus, if

$$W = W_0 = \text{const}, \tag{3}$$

the rupture is forced to propagate in a relatively thin brittle layer.

We use notation m for the moment magnitude:

$$m = \frac{2}{3}\log_{10} M - 6, \tag{4}$$

where M is measured in N m. The magnitude calculated by (4) is used here only for illustration, all pertinent computations being carried out with the moment M values.

Although other geometrical parameters of earthquake rupture have been correlated with seismic moment, the length of the rupture is determined with significantly better accuracy than width or slip. This is reflected, for example, in a higher correlation coefficient of M versus l compared to the correlation of the moment with W or u (Wells and Coppersmith, 1994): $\rho = 0.95$, 0.84, and 0.75, respectively. Thus, we only use the M versus l correlation in this study.

There is a significant amount of literature on the scaling relation of the aforementioned variables for various faults and earthquakes (Kanamori and Anderson, 1975; Geller, 1976; Sato, 1979; Romanowicz, 1994; Wells and Coppersmith, 1994; Abercrombie, 1995; Pegler and Das, 1996; Scholz, 1997, 1998; Bodin and Brune, 1996; Wang and Ou, 1998; Mai and Beroza, 2000; Stock and Smith, 2000; Fujii and Matsu'ura, 2000; Shaw and Scholz, 2001, and references therein). Abercrombie (1995) showed no slope break in composite data sets for small and moderate earthquakes and a slope of 3, albeit with a large scatter. Although the scaling exponent $d = 3$ for $m \leq 6$ events is now generally accepted, various empirical and theoretical values for d have been proposed for larger earthquakes: $d = 1.0$, 1.5, 2.0, and 3.0.

Two models have been proposed for scaling of slip in large earthquakes: the W-model (Romanowicz, 1994, and

references therein), which assumes that slip is proportional to the rupture width W and consequently is constant as long as condition (3) holds. A second model, called the L-model (Scholz, 1997; 1998, and references therein), assumes that $u \propto l$. Assuming that fault width is essentially constant, as discussed previously, the W-model predicts $d = 1$, whereas the L-model requires $d = 2$. Various empirical data have been used to confirm or refute the aforementioned hypotheses. Because of the poor quality of the data and inappropriate control over data selection, the results have been inconclusive.

Two problems are obvious in previous solutions of the earthquake scaling relation: (1) Statistical techniques: Many magnitude estimates are derived from intensity data or from other less-than-reliable sources. Since their accuracy is low, one must take into account uncertainty in both magnitude and rupture length. (2) Data: As Pegler and Das (1996) suggest, data on rupture length come from different, sometimes unreliable sources that often yield multiple solutions. The accuracy, systematic errors, and selection biases of each length and magnitude determination are not well controlled.

Wang and Ou (1998) reanalyzed the data of Wells and Coppersmith (1994). In addition to the ordinary least-square regression (moment versus length) they used the major-axis least-squares method, which assumes that both regression variables have an associated experimental error. For the ordinary least-squares the value of the d exponent is 2.2–2.5, but it increases to 2.4–3.0 when the more appropriate (major-axis) method is used.

Stock and Smith (2000) analyzed a set of 550 earthquake scaling data that included the Wells and Coppersmith (1994) list. They also took into account uncertainties in both variables. They obtained $d = 3$ scaling for all earthquakes other than large strike-slip events ($M > 10^{19}$ N m), for which they suggest $d = 2$ as a more appropriate scaling. Their data set contains 14 strike-slip earthquakes with $M \geq 10^{20}$ N m ($m \geq 7.33$), most of which form a point cloud, justifying the approximation $d = 2$ for large earthquakes. However, on closer inspection the list reveals that all but one (the 16 July 1990 Philippines) earthquake occurred before 1977 (the Nobi, Japan, earthquake time is 28 October 1891, not 28 October 1981). Thus, almost all the large strike-slip earthquakes on their list are from a predigital or even preinstrumental era, so the scalar moment values were determined with a large error. For preinstrumental earthquakes, the moment value is usually calculated by assuming a W value in (1) equal to 15 or 20 km. Thus, the scaling break is, in effect, postulated. Surface-wave M_S and body-wave m_b magnitudes saturate for large earthquakes, hence predigital but instrumental results are also not very reliable for the largest events. Therefore, the largest old earthquakes data may be biased.

Pegler (1995) and Pegler and Das (1996) obtained a distribution of rupture length scaling for strike-slip earthquakes using systematically uniform unbiased selection criteria and modern interpretation methods. Their data set, which extends to moments larger than 10^{21} N m and rupture lengths in excess of 200 km, contains no visual trace of the scaling break (see also Scaling Regression Fit section). Although Pegler and Das (1996) propose that exponent $d = 2$ explains their results, it is obvious from their figure 1b that a more gradual regression line should be employed. In a later analysis of these and additional aftershock data, Henry and Das (2001) suggest that a line with the exponent $d \approx 2.7$ is the best fit for strike-slip earthquakes. In the Scaling Regression Fit section, we reinterpret Pegler and Das (1996) data.

In this work we assume that the length of the aftershock zone is proportional to the length of the mainshock rupture. We analyze aftershock sequences in a uniform formal manner to determine their scaling relations. Simultaneously, we try to avoid various systematic effects and biases by applying consistent criteria for data selection and studying the effect of these criteria on obtained results.

Data and Technique

Earthquake Catalogs

For our study of aftershock distribution, we take mainshocks from the global catalog of centroid moment tensor (CMT) inversions compiled by the Harvard group (Dziewonski *et al.,* 2001). The catalog contains 16,598 solutions over a period from 1 January 1977 to 31 December 2000.

The aftershocks are collected from the Preliminary Determination of Epicenters (PDE) (NEIC) worldwide catalog of earthquakes (Preliminary Determination of Epicenters, 2000) that ends on 1 January 2001. The catalog measures earthquake size, using several magnitude scales, of which m_b and M_S are provided for most moderate and large events.

Procedure

Pegler and Das (1996) relocated all aftershocks in their study using International Seismological Center (ISC) phase-arrival data. Such relocation should on average decrease location errors. However, in addition to the significantly increased effort needed to reinterpret the data, a drawback occurs in such a procedure, which is rarely mentioned in research literature. If investigators prepare data for statistical analysis, there is an increased possibility that both intentional and inadvertent bias may be introduced in the data. Selection of data processing methods, details of techniques, choice of input raw data, and so forth, can influence the final results in a manner that would be difficult to account for. Many relocation techniques, such as the Joint Hypocenter Determination technique, introduce statistical dependence in location errors, since location errors of each aftershock would in a hidden form contain the master event error. Depending on the technique applied, this dependence may make the final statistical analysis questionable. In addition, data processing details are so difficult to communicate fully that the results of such efforts are largely nonreproducible. Reproducibility of an experiment or an observation is an

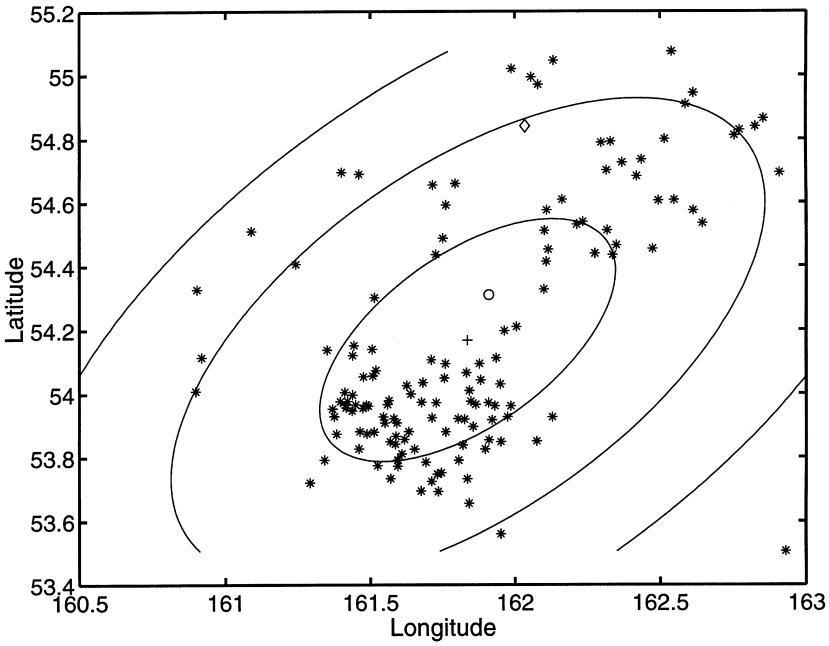

Figure 1. Aftershock map for 5 December 1997 Kamchatka earthquake (M 5.32 $\times$ 10^{20} N m, m 7.82). Stars, aftershock epicenters; cross, average aftershock position; circle, centroid vertical projection onto the Earth surface; diamond, NEIC mainshock epicenter. Two-dimensional Gaussian approximation of aftershock distribution is shown, and ellipses are drawn at 1σ, 2σ, and 3σ levels.

important part of the scientific method. Thus, to make our results easily replicated, we accept as raw data source coordinates and earthquakes size characteristics (the scalar seismic moment and magnitude) given in the above catalogs. However, we also explore how earthquake location errors affect our results.

The broad outline of our procedure follows:

1. Any large earthquake in the Harvard CMT catalog is considered a mainshock.
2. We designate all earthquakes within a specific time-distance window occurring after a mainshock as an aftershock sequence. Since there are no widely accepted criteria for defining the aftershock zone, we take several reasonable choices for window parameters and demonstrate that the results are largely independent of that selection.
3. An ellipsoidal area is fitted to the spatial distribution of the aftershock sequence.
4. Ellipse parameters are statistically analyzed to find scaling characteristics.

Our aim is to discuss the principles of data selection and then present how we processed the data (see the following section and, in particular, its last paragraph for the preferred choices). We also investigate some variations from the preferred set. The Aftershock Pattern section presents the statistical techniques for the analysis.

To illustrate the subsequent discussion of the data selection and processing, Figure 1 displays an aftershock area for the Kamchatka earthquake 5 December 1997 and its fit by a two-dimensional Gaussian (binormal) distribution. Three ellipses are plotted, corresponding to 1σ, 2σ, and 3σ confidence areas. The probability that a point is inside a k-σ ellipse follows the Rayleigh or the the chi-square with two degrees of freedom [$\chi^2(2)$] distribution. The probability is calculated as

$$\text{Prob} = 1 - \exp\left(-\frac{k^2}{2}\right). \tag{5}$$

This probability is smaller than that for the one-dimensional Gaussian distribution: the 2σ probability is 0.86 instead of the familiar 0.95 for the one-dimensional case (see, for example, Press *et al.,* 1992, pp. 688–689). However, we usually are more interested in the aftershock distribution projected on the major ellipse axis; since this marginal distribution is one-dimensional Gaussian, the one-dimensional approximation can be used.

The fit of the aftershock pattern by the Gaussian distribution cannot be exact. First, some aftershocks occur at large distances from the mainshock where no other traces of earthquake rupture can be found, as the 1992 Landers, California, aftershock sequence (Hill *et al.,* 1993) demonstrated. Second, aftershocks exhibit the feature of secondary clustering, strong aftershocks forming centers of densely concentrated new events. Thus, statistically, aftershocks are not mutually independent in space.

Moreover, the traditional classification of earthquakes into mainshocks/aftershocks is itself a rough approximation. In such an approach, earthquakes are treated as mutually independent points in space and time. In reality, even large earthquakes are accompanied by even stronger events, sometimes well separated in time and space, sometimes not (Kagan and Jackson, 1999). Aftershock sequences of such mainshocks may intersect, making ambiguous the definition of the focal area. The only appropriate way to resolve these

difficulties is by applying stochastic point processes to analyze earthquake occurrence (Kagan, 1991; Kagan and Jackson, 2000; Ogata, 1998). However, such an analysis requires much more effort; its results are not easy to comprehend and may be subject to biases that are too difficult to estimate. Thus, this work relies upon simpler procedures to evaluate earthquake scaling properties.

Data Selection

Several choices need to be made when selecting and processing data:

1. When fitting a regression line, we may assume uncertainty only in l, or assume that both regression variables have comparable accuracy.
2. A minimum number of events in aftershock sequences (N_a) needs to be specified. Ogata (1998, p. 393) suggests using $N_a = 6$ when approximating aftershock spatial distribution by the two-dimensional Gaussian law. Below we use two choices $N_a = 5$ and $N_a = 10$.
3. In selecting aftershock sequences, a time-distance window can be centered on an epicentroid or on the middle point of the sequence. (We define *epicentroid* as the vertical projection of the moment centroid onto the surface of Earth.) Thus, in the latter case we make a two-step selection: first to identify the middle point and then to look at earthquakes around this point.
4. The maximum distance over which aftershock sequences are selected (r_m) and its parametrization vary. Some guidance can be obtained from the results of the likelihood analysis of earthquake catalogs (Kagan, 1991; Kagan and Jackson, 2000). In these studies we approximate the spatial distribution for dependent earthquakes by a Gaussian distribution isotropic in space with a standard error 9.5 km for a m 7 earthquake. But the real distribution of aftershocks is anisotropic, extended along a mainshock fault plane. Thus, we should expect the major ellipse axis to be larger than the previous value and the minor axis to be smaller. Moreover, the aftershock distribution depends on the type of earthquake mechanism, tectonic environment, and other factors, so the best approach would be to determine the spatial parameters once again. One possibility is to use one distance for earthquakes of all sizes; another is to make the distance dependent on the mainshock magnitude. The former choice has an advantage of imposing less prior restriction on scaling parameters. However, some distant aftershocks or independent events, occurring by chance within a window, may bias the results.
5. Depth limit for mainshocks and aftershocks can be selected as $D = 0$–70 km or $D = 0$–35 km. It is possible to use the same depth range for both sets of earthquakes or select aftershocks having a prescribed depth difference.
6. To define the time span for an aftershock sequence (ΔT), we can use either 1-day (as in Pegler and Das, 1996) or 7-day limits. Taking a smaller time span would diminish the number of aftershock sequences available for the analysis, whereas using longer intervals means that more sequences would overlap and complicate the analysis.
7. Should all earthquakes in the Harvard list above a certain moment limit be considered as mainshocks, or should the events close in time and space, that is, potential aftershocks or foreshocks themselves, be excluded? (See the last paragraph of the Procedure section). To test the influence of closely occurring mainshocks, in one case we removed all events separated by less than $2\Delta T$ from the CMT catalog, that is, two days.
8. We may take an aftershock location as given by the catalog, or we can take into account their possible location errors when calculating scaling relations.

We explore these possibilities in Table 1. The numbers in the table correspond to the numbers in the previous list. In addition to the aforementioned choices, some other conditions need to be specified. For most we did not explore alternative possibilities, but for the sake of completeness list them below:

9. A lower moment or magnitude threshold for mainshock selection is another option. (We use $m \geq 7.0$ consistently in this work. When calculating the moment magnitude (see equation 4), we take the scalar moment value from the Harvard CMT catalog corresponding to the double-couple source.) The source areas of these earthquakes are significantly larger than location errors. If we were to select smaller mainshocks for the analysis, it would be difficult to exclude influence of the location errors, and the results would become less reliable. The total number of such shallow (depth 0–70 km) earthquakes in the 1977–2000 Harvard catalog is 231; thirteen of them have $m \geq 8.0$.
10. A lower magnitude threshold for aftershock selection is also an option. We use earthquakes with a body-wave magnitude $m_b \geq 4.5$ because this magnitude is most consistently provided by the PDE catalog. Although earthquakes above this threshold value may not be uniformly sampled over the spatial and temporal extent of the catalog, we feel that the catalog inhomogeneity would have only a minor effect on results.
11. Epicenters or hypocenters can be used in determining distance.
12. A probability density threshold selection needs to be made to define the mainshock focal area. After fitting an aftershock spatial pattern with a two-dimensional Gaussian distribution, we select the level (for example, 2σ or 3σ) at which the zone size is defined.
13. Finally, although it is usually assumed that the scaling dependence between moment and earthquake focal area size (l) is linear in log–log scale, various factors can make this dependence nonlinear. Thus, we can approximate such dependence by either the linear regression, or, for example, a quadratic polynomial formula.

Table 1
Values of Parameters for Earthquake Focal Zone Distribution*

#	Earthquakes: Case	All n	All a_1	All L	Thrust n	Thrust a_1	Thrust L	Normal n	Normal a_1	Normal L	Strike-Slip n	Strike-Slip a_1	Strike-Slip L
0	Standard	91	.47	2.47	64	.47	2.45	8	.52	2.44	19	.46	2.52
1	Both err., $\lambda = 0.25$	91	.49	2.48	64	.49	2.47	8	.53	2.45	19	.47	2.49
2	$N_a = 5$	144	.47	2.45	99	.46	2.44	13	.52	2.45	32	.44	2.47
3	Aft.-center.	93	.49	2.46	67	.46	2.45	8	.52	2.44	18	.56	2.54
4	$r_m = 500$ km	95	.39	2.50	68	.43	2.52	8	.32	2.40	19	.30	2.50
5	D = 0–35 km	71	.47	2.47	49	.48	2.46	8	.52	2.45	14	.38	2.49
6	$\Delta T = 7$d	133	.43	2.45	95	.40	2.42	12	.61	2.57	26	.40	2.46
7	Close del.	75	.50	2.47	49	.51	2.46	8	.52	2.44	18	.49	2.55
8	$\varepsilon = 7.5$ km	91	.51	2.48	64	.52	2.47	8	.57	2.45	19	.49	2.53

*n is the number of aftershock sequences; a_1 is the coefficient of linear regression in (16); and L is the decimal logarithm of the aftershock some length (14) for a mainshock of magnitude 8.25 (seismic moment $10^{21.375}$ N m). The values of linear regression coefficients (a_1) are listed for several selections of aftershock sequences accompanying large ($m \geq 7$) earthquakes. See Data Selection section for explanations of cases; the numbers in the first column correspond to item numbers in this section.

Some of the aforementioned selection criteria are relatively easy to test. For example, we found that for mainshocks with the moment greater than $10^{19.5}$ N m and depth limits 0–70 km, there is little difference in using hypocentral or epicentral distances. In regard to the depth range selection (item 5), it is also moot whether we use common limits for both sets of the events or select aftershocks within a 35-km range of the mainshock depth. To study the influence of other selections, we designate one case as standard and compare the other selection choices.

In the standard case, we assume that only the length l is determined with an error and center our aftershock selection window on the epicentroid. We treat all $M \geq 10^{19.5}$ N m ($m \geq 7$) earthquakes in the Harvard list as potential mainshocks and do not take into account aftershock location errors. We use $N_a = 10$ and $D = 0$–70 km for both mainshocks and aftershocks, $\Delta T = 1$ day, and

$$r_m = 20 \times 10^{(m-6)/2} \text{km}. \tag{6}$$

The standard case list of mainshocks and parameters of their aftershock sequences (the appendix) can be downloaded from *http://moho.ess.ucla.edu/kagan/aftershocks.txt.* Possible deviations from the standard case and results are shown in the Results section Table 1.

Aftershock Pattern

We categorize earthquakes according to the prevalent focal mechanism: thrust, strike slip, and normal. For example, an earthquake is considered to have a normal focal mechanism if its most-compressive principal axis of the moment tensor (P axis) is more vertical than either the principal axis B or T (Frohlich, 2001). Similarly, we define earthquakes with the thrust and strike-slip mechanism when the T axis or B axis is more vertical than others, respectively.

To define an earthquake focal area, we employ a formal quantitative algorithm, approximating the aftershock set by a two-dimensional Gaussian distribution. The probability density contours of such a distribution are ellipses. We take the major axis of the ellipse as a measure of the earthquake rupture length. Utsu (1969) suggests that, since small mainshocks have on average fewer aftershocks, regression results may be biased. This bias should be especially strong if one evaluates an aftershock zone size by visual inspection. Employing a quantitative statistical estimation excludes this bias, although, the accuracy of the zone-size determination would of course depend on the available number of events.

To obtain the distribution parameters for an aftershock sequence of N events, we first calculate sums

$$[xx] = \sum_{i=1}^{N} (x_i - \bar{x})^2, \tag{7}$$

$$[yy] = \sum_{i=1}^{N} ((y_i - \bar{y})\cos(\bar{x}))^2, \tag{8}$$

and

$$[xy] = \sum_{i=1}^{N} (x_i - \bar{x})(y_i - \bar{y})\cos(\bar{x}), \tag{9}$$

where x_i is the latitude, y_i is the longitude of ith aftershock, $\bar{x}$ is the average latitude for the aftershock sequence, and $\bar{y}$ is the average longitude. Since the distances over which sequences are considered are less than 500 km, we use simplified formulas (cos ($\bar{x}$) in equations 8 and 9) to calculate them.

Subsequently, we calculate the correlation coefficient ρ_a, which shows a tilt of the ellipse versus the coordinate axes, and the major σ_j and minor σ_n semiaxes of the ellipse.

$$\rho_a = \sqrt{\frac{[xy]}{[xx][yy]}}, \tag{10}$$

$$\sigma_j^2 = \frac{1}{2(N-1)}\left([xx]+[yy]+\sqrt{([xx]-[yy])^2+4\rho_a[xx][yy]}\right), \quad (11)$$

$$\sigma_n^2 = \frac{1}{2(N-1)}\left([xx]+[yy]-\sqrt{([xx]-[yy])^2+4\rho_a[xx][yy]}\right), \quad (12)$$

In further analysis, the length of the mainshock focal zone is given as

$$l = 4\sigma_j, \quad (13)$$

that is, as the length of the 2σ confidence area (the second ellipse in Fig. 1). We denote the decimal logarithm of l as

$$L = \log_{10} l. \quad (14)$$

The previous definition of the zone length assumes that the major axis is parallel to the Earth's surface. If fault planes are dipping, the axis may not be horizontal. However, as our tests (see following paragraph and item 13 in the previous list) show, using the three-dimensional determination of distances changes no conclusions.

Results

Aftershock Pattern Phenomenology

Figures 2–4 explore the phenomenology of aftershock sequences. In these and in the rest of the plots we employ the least-squares technique to approximate dependence between two variables. We approximate it either by a linear regression or a quadratic polynomial formula. The behavior of the dependence for the largest earthquakes has the greatest interest where the influence of location and other errors is smaller. Furthermore, as mentioned in the Introduction, the scaling of these largest earthquakes stimulates the most controversial discussion. Therefore, in regression curves we use as a reference point m 8.25; the new, shifted variable is denoted as $m_r = m - 8.25$. An additional advantage of such a shift is that, if the quadratic fit is significantly better than the linear regression, the a_1 coefficient in (16) shows the actual exponent value at m 8.25. Similarly, when using the opposite regression, i.e., magnitude against log length, we shift the length reference point toward large values: $L_r = L - 2.5$.

$$m_r = a_0 + a_1 L, \quad (15)$$

$$m_r = a_0 + a_1 L + a_2 L^2, \quad (16)$$

$$L_r = b_0 + b_1 m, \quad (17)$$

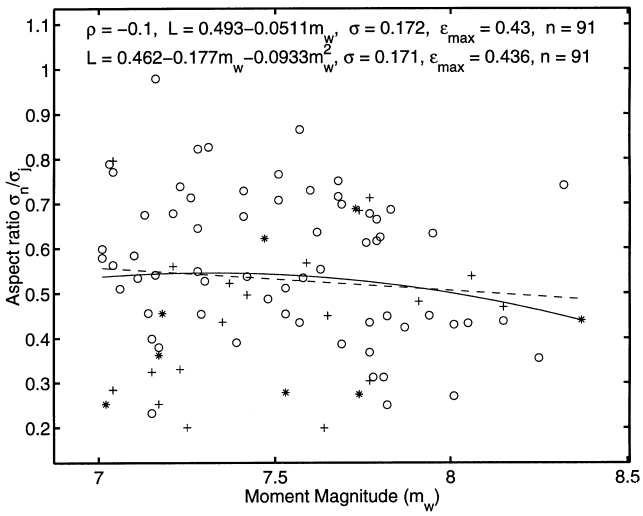

Figure 2. Aspect ratio minor to major axes (σ_n/σ_j) for aftershock sequence pattern and its dependence on moment magnitude. Correlation coefficient (ρ) and linear and quadratic regression coefficients are shown, as well as the standard (σ) and maximum (ε_{max}) errors and total number of sequences (n). The dashed line is the linear regression, and the solid line is a quadratic approximation. Circle, thrust mainshocks; star, normal mainshocks; plus, strike-slip mainshocks.

$$L_r = b_0 + b_1 m + b_2 m^2. \quad (18)$$

The standard deviation of regression curves provides the uncertainty estimate for the fit, a rather insufficient one in our case. The reason for this is that the distribution of variables, especially the distribution of earthquake size, is non-Gaussian. The seismic moment is distributed according to the power law; the Gutenberg–Richter relation is a logarithmic transformation of the law (Kagan, 2002a). In our plots, not all mainshocks are included, only those satisfying the outlined conditions. The size distribution of selected mainshocks may differ from the Gutenberg–Richter law but is clearly much different from the Gaussian distribution. As Press *et al.* (1992) indicated, for highly non-Gaussian variables, the results of regression are often questionable. Thus, this work deemphasizes formal statistical tests and pays more attention to the consistency of the results.

Taking the above into account, we calculate the standard deviation (σ) and standard error (σa_1) of a_1 parameter estimates. These σ estimates yield at least an approximate measure of error and can be considered as a lower bound of real uncertainties.

$$\sigma^2 = \frac{[xx][yy]-[xy]^2}{n[xx]}, \quad (19)$$

where $[xx]$, $[yy]$, and $[xy]$ are defined similarly as in (4), n is the number of aftershock sequences, and

$$\sigma_{a1}^2 = \frac{n\sigma^2}{(n-2)[xx]}. \quad (20)$$

Figure 2 displays the aspect ratio (σ_n/σ_j) for the ellipses approximating the aftershocks' spatial pattern. Obviously the ratio either does not depend on the earthquake size at all or has a weak dependence with stronger earthquakes exhibiting slightly smaller ratios. If the epicenter positions are perturbed by location errors, these errors increase the ellipse minor axis to a relatively larger degree for smaller earthquakes. There is no significant difference between the earthquakes of various focal mechanisms.

Figure 3 shows the distance between the center of the aftershock area and the mainshock epicentroid versus the earthquake size. In general, these two variables should not coincide. Because the catalog compilers use different methods to construct hypocenter and centroid and a different Earth structure, their systematic errors vary (Smith and Ekström, 1997). Conversely, the distance should not depend on the earthquake magnitude because the systematic effects in both catalogs are not obviously connected to earthquake size. The diagram shows that any correlation between the distance and moment magnitude is low, and distance increases only slightly with magnitude.

Figure 4 explores another aspect of the interrelation of two catalogs: the dependence of mainshock epicenter–epicentroid distance on the earthquake size. The epicenter marks the point where an earthquake rupture begins, whereas the centroid corresponds to a gravity center of the seismic moment release. The hypocenter is usually located at some distance from the centroid. The location difference is due to location errors and to rupture originating closer to the focal area edge (Smith and Ekström, 1997). For larger earthquakes, the distance between these two points should on average increase, as the diagram weakly displays.

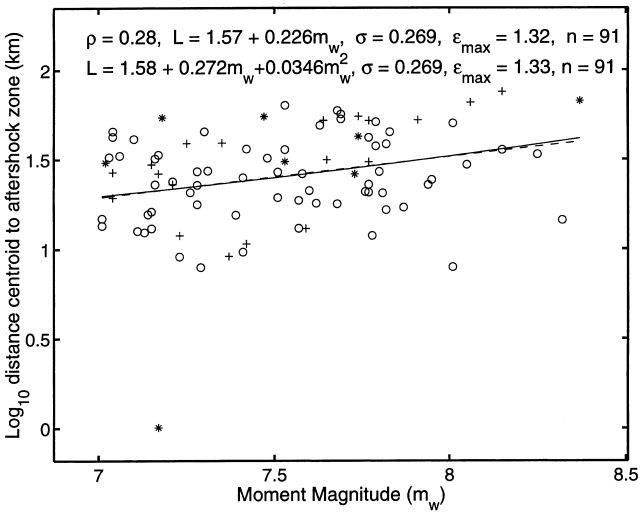

Figure 3. Dependence of the distance between the aftershock area center and a mainshock epicentroid. All symbols are similar to Figure 2.

Scaling Regression Fit

Figure 5 displays Pegler and Das's (1996) results (taken from their table 1) with linear and quadratic regression approximations, as shown in equations (15) and (16). In this

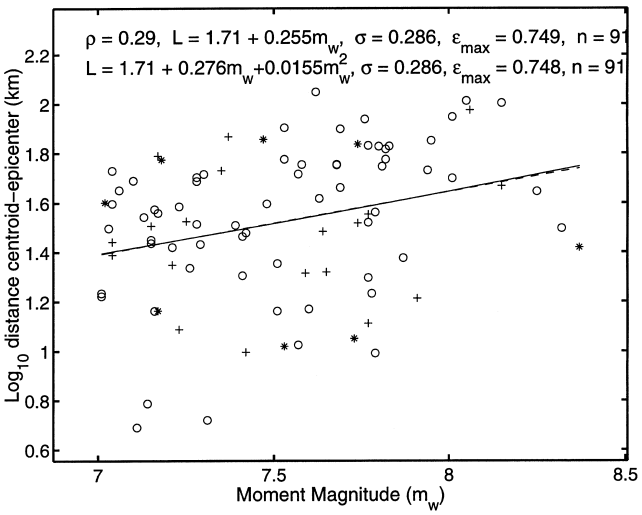

Figure 4. Dependence of the distance between the mainshock epicenter and an epicentroid. All symbols are similar to Figure 2.

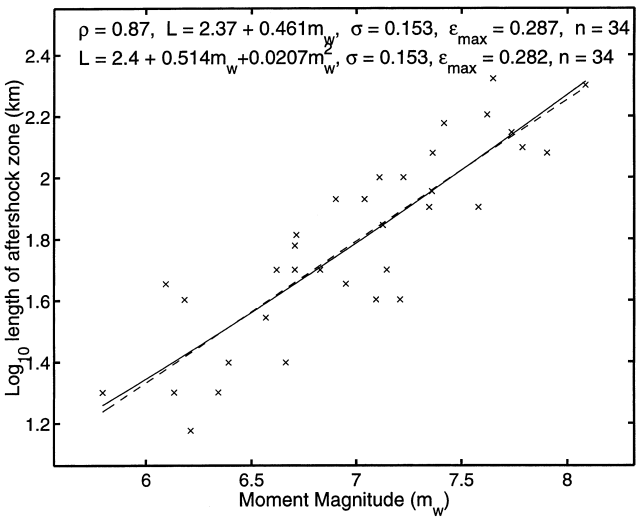

Figure 5. Plot of log aftershock zone length (L) versus moment magnitude (m) for strike-slip earthquakes studied by Pegler and Das (1996, their table 1). Magnitude values are shifted in formulas shown in the plot ($m_r = m - 8.25$). Rupture length is determined using a 1-day aftershock pattern. Values of the coefficient of correlation (ρ), coefficients for linear (dashed line) and quadratic (solid line) regression, standard (σ) and maximum (ε_{max}) errors, and the total number (n) of aftershock sequences are shown in diagram.

plot we assume that only L is determined with an error. The inspection of the plot demonstrates that the linear regression matches the data well. Leonard *et al.* (2001) obtained a similar result: the linear fit model is not rejected when compared to a change-point model, that is, the regression with two straight lines. For the linear regression log aftershock length versus log moment (opposite to the regression in our Fig. 5), they obtained $d \approx 2.4$ (their figure 4b). Since the log length is determined with a higher error than the seismic moment, as we see in the following section, their d value is estimated with a significant negative bias.

The slope of the line 0.46 in Figure 5 needs to be divided by 1.5 to obtain $1/d$, the value of the scaling exponent:

$$d = \frac{1.5}{a_1}. \tag{21}$$

For small values of the ratio σ_{a1}/a_1, its standard deviation is

$$\sigma_d \approx \frac{1.5\sigma_{a1}}{a_1^2}. \tag{22}$$

The d value for the linear regression is 3.25 ± 0.34; thus the exponent value $d = 3$ is within the 1σ confidence interval. But the d value of 2.0 falls clearly outside the confidence limits. If the saturation effect (the d value decrease) for the largest earthquakes is present in the data, the quadratic correction coefficient should be positive, as in the diagram. However, the value of the slope at m 8.25 is 0.514, corresponding to $d = 2.9$. Moreover, the standard deviation (σ) value is practically the same for the linear and quadratic regressions. Since the latter regression employs an additional degree of freedom, any statistical test would reject the quadratic regression as an appropriate fit to the data.

In Figure 6a–d we display the regression curves for Harvard/PDE earthquakes in the same format as in Figure 5: all earthquakes are taken together and separately for three choices of focal mechanisms. In all diagrams the standard errors (σ) are almost the same for the linear and quadratic regression; the maximum errors ($\varepsilon_{\max}$) follow the same pattern. As explained in the previous paragraph, this signifies that the linear regression is sufficient to approximate the data. Although the quadratic regression fit yields no statistically significant improvement in any diagram, for the first three data sets, the sign of the quadratic correction term is negative. Thus, the d value increases at the high magnitude end, and no saturation effect occurs in the data.

As discussed in the Introduction, very large strike-slip earthquakes are expected to exhibit a saturation effect (see Stock and Smith, 2000, for more explanations). Although the sign of the quadratic correction term for these earthquakes is positive, this effect is caused by just one event—the Antarctic (Balleny Islands) 25 March 1998 earthquake. Toda and Stein (2000) noted that the exceptionally long aftershock area for this earthquake is over 350 km. Antolik *et al.* (2000) also suggest that the aftershock zone is about 300 km long. Henry *et al.* (2000) argued that the mainshock consisted of at least two subevents whose rupture planes are separated by about 100 km. However, their moment tensor solution significantly differs from that in Antolik *et al.* (2000). McGuire *et al.* (2000) analyzed this earthquake, using higher-order seismic moment tensor formalism, and obtained an estimate for a focal zone length 178 ± 46 km.

Although it is common when interpreting new data to obtain different solutions due to the nonunique inversion and varying assumptions, it is very important, as remarked in the Introduction, that all data used in statistical analysis be processed by an identical technique. Otherwise, a selection bias would be practically unavoidable.

In general, most earthquakes have a complex internal temporal and spatial structure that is not considered here. In our calculations, the 25 March 1998 earthquake has the longest focal zone of all mainshocks, $4\sigma_j$, around 461 km (see the Appendix). Without this earthquake, the values of the regression coefficients for strike-slip events are $a_1 = 0.38$ in the linear case and $a_2 = -0.23$ in the quadratic.

For earthquakes of different focal mechanisms, no significant difference occurs in the data-point pattern or the values of the regression parameters: the correlation coefficient, the value of the L intersect at m 8.25, and the slope of the line are approximately the same for all earthquake sets. We compute standard errors for linear regression parameters: $d = 3.17 \pm 0.25$, $d = 3.17 \pm 0.29$, $d = 2.86 \pm 0.36$, and $d = 3.28 \pm 0.69$, for all events, thrust events, normal events, and strike-slip events, respectively. Again, as in Figure 5, $d = 3$ is within the 1σ confidence limits for all earthquake sets. The uncertainty in the d value is relatively high because of the small magnitude range in our plots.

Similarly, we calculate the standard deviation for the a_0 value: $\sigma a_0 = 0.030$, 0.035, 0.054, and 0.079, respectively. The intersect value (a_0) is similar (2.45–2.50) for all diagrams; thus an m 8.25 earthquake of any focal mechanism ruptures about 300 km on average. This value generally agrees with our previous determination of spatial earthquake scatter (Kagan, 1991; Kagan and Jackson, 2000). For a m 7 earthquake, $\sigma j \approx 18$ km (6), which exceeds the isotropic estimate by a factor of 2 (see Data Selection section, item 4), this difference is expected for a major ellipse axis versus the radius of a circle in approximating an aftershock pattern. Pegler (1995) and Pegler and Das (1996) data (see Fig. 5) suggest a slightly smaller value for $a_0 = 2.4$, corresponding to about a 250-km rupture length. However, their l definition appears to differ from ours.

If we put the a_0 values from our regression plots (m 8.25, $l \approx 300$ km) into Figure 11 by Abercrombie (1995), they all match the composite plot at the stress drop value of about 0.3 MPa, slightly lower than most other points. Similarly, our data, if plotted in Stock and Smith (2000, their figures 2–4) diagrams, would correspond to higher L values than most of their entries. However, in these publications the data points for earthquakes are obtained using different for-

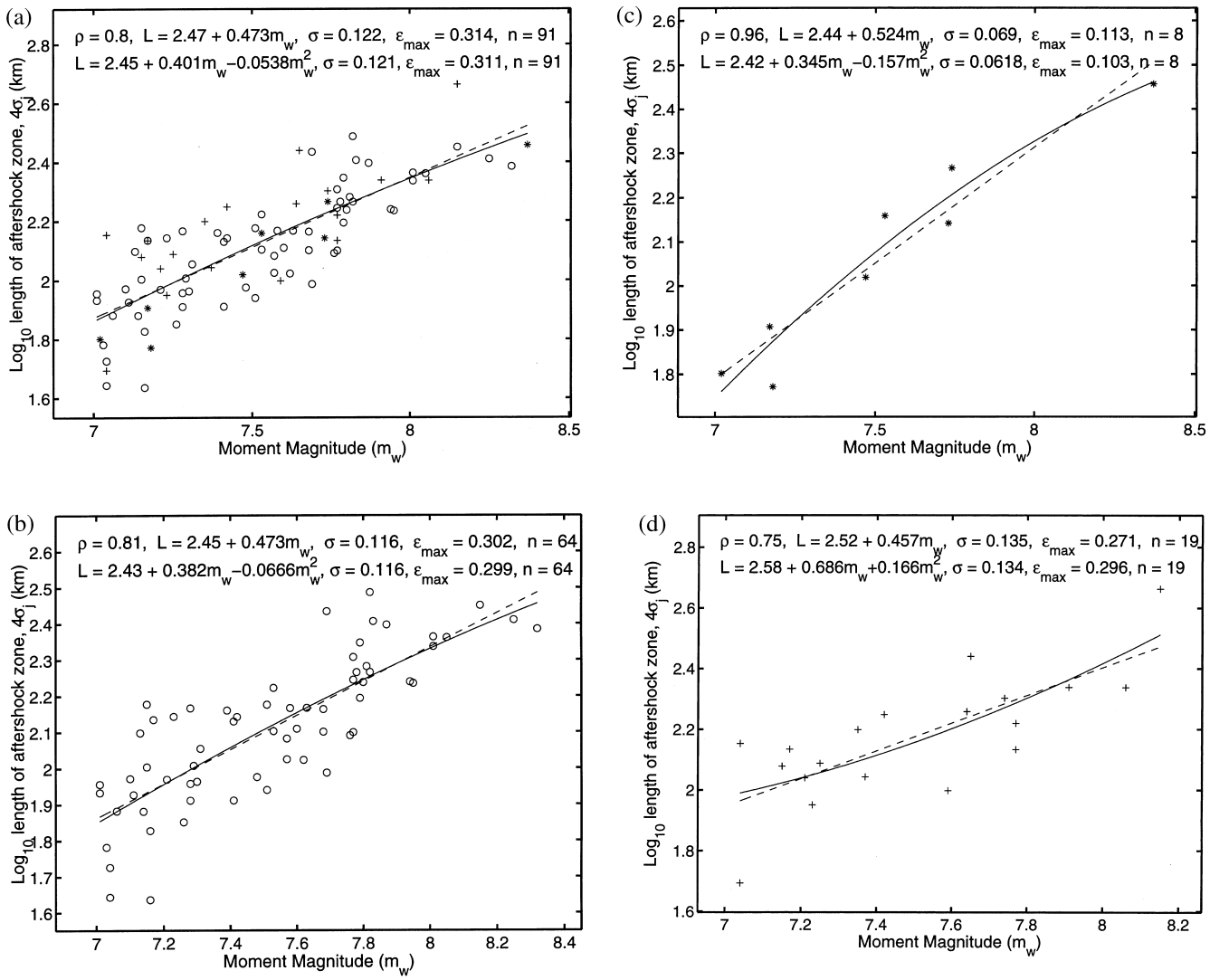

Figure 6. Plot of log aftershock zone length (L) against moment magnitude (m). Magnitude values are shifted in formulas shown in the plot ($m_r = m - 8.25$). Rupture length is determined using a 1-day aftershock pattern. Values of the correlation coefficient (ρ), coefficients for linear (dashed line) and quadratic (solid line) regression, standard (σ) and maximum ($\varepsilon_{\max}$) errors, and the total number (n) of aftershock sequences are shown in diagram. (a) All earthquakes, symbols are similar to Figure 2; (b) thrust earthquakes; (c) normal earthquakes; (d) strike-slip earthquakes.

mal or often informal criteria for earthquake source region determination. For instance, if 1σ ellipse (see Fig. 1) is taken as the source zone definition, our results would fit in the middle of Abercrombie (1995) or Stock and Smith (2000) data points. Without significant effort it is difficult to resolve how our 2σ source specification relates to other determinations of the focal zone. Thus, comparison with other results suggests that the $d = 3$ scaling would match the data for all magnitudes and focal mechanisms.

Figure 7 displays the regression fit opposite to Figure 6: we assume that the uncertainties are only in determining magnitude. The standard deviation of the fit here is much higher than in Figure 6, and the quadratic regression often significantly differs from the linear, especially for earthquakes of different focal mechanisms (separate plots are not shown here to save space). If we calculate the d value using the linear fit, $d = 1.34 \times 1.5 = 2.01$, that is, a much smaller estimate than we obtain in Figure 6. The reason for such a bias is obvious: errors are much higher for L than for m (see also the first paragraph of Scaling Regression Fit).

Uncertainties and Parameter Variations

The standard errors shown in Figures 6 and 7 are measured along a vertical line because we assume that the abscissa values are measured with no error. In each case, a scatter of data points is significantly higher along the magnitude axis than along the log aftershock area length axis.

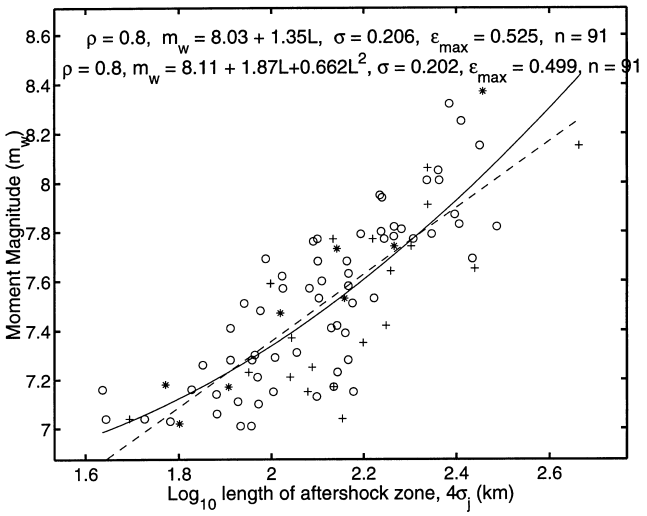

Figure 7. Plot of moment magnitude (m) versus log length of aftershock zone (L). Log length (L) values are shifted in formulas shown in the plot ($L_r = L - 2.5$). All symbols are similar to Figure 2.

This implies that the log aftershock length is more inaccurate than the moment magnitude.

We would like to estimate how accurate the measurements of both variables in Figure 6 are to see whether the least-squares method in which both variables have an uncertainty should be used, and, if necessary, to evaluate these errors ratio. To do this, we determine the major and minor axes of the ellipse using equations (10)–(12). For the minor semiaxis (σ_n) the values of 0.06–0.12 are obtained. These values are close to the standard errors shown in Figure 6, confirming that measuring the aftershock area size mostly contributes to the total uncertainties in the regression.

A square of the value of the minor semiaxis is approximately equal to the variances sum of both variables (York, 1967):

$$\sigma_n^2 = \sigma_m^2 + \sigma_a^2, \tag{23}$$

where σ_m is the uncertainty in the measurement of the moment magnitude, and σ_a is the standard deviation in the log length for an aftershock zone. The σ_m estimate can be obtained by comparing the moment values in the catalogs of moment solutions. For example, with shallow earthquakes the standard deviation for the $\log_{10}(M)$-difference in the Harvard and U.S. Geological Survey (USGS) (Sipkin *et al.,* 2000, and references therein) catalogs is about 0.1 (Helffrich, 1997; Kagan, 2002a).

If we assume that the Harvard solution variance is equal to that of the USGS solution, then the uncertainty (σ_1) in $\log_{10}(M)$ is

$$\sigma_1 = \frac{0.1}{\sqrt{2}}, \tag{24}$$

and the standard error for the moment magnitude determination

$$\sigma_m = \sigma_1 / 1.5 = 0.047. \tag{25}$$

Taking $\sigma_n = 0.09$ (see the second paragraph), we calculate the variances ratio value λ

$$\lambda = \sigma_m^2 / \sigma_a^2 \approx 0.25, \tag{26}$$

which is necessary to estimate the regression if both variables have errors (York, 1966; 1967; Press *et al.,* 1992, p. 660; Stock and Smith, 2000). The λ value is smaller than $\lambda = 0.5$, assumed by Stock and Smith (2000). It is not surprising since most earthquakes in their data set are from the predigital era and hence have large magnitude errors. In our plots σ_n is usually larger than 0.09. Moreover, as Figure 5 in Kagan (2002a) demonstrates, the magnitude errors are smaller for large earthquakes, possibly by a factor of 2. Consequently, the λ value is, most probably, significantly smaller than 0.25, and the magnitude uncertainty for the Harvard CMT data can be ignored.

It is likely that most uncertainty in the aftershock zone size is caused not by the location and other errors of seismogram processing, but rather by the natural randomness of earthquake occurrence and stochastic scatter of aftershock locations. Thus, even in local catalogs for which seismogram interpretation errors are significantly lower than those of global catalogs, σ_a values can still be comparable to our estimates.

We use $\lambda = 0.25$ to evaluate regression coefficients. As shown in Table 1 (row 2), even for this certainly high λ value, the two estimates (the standard case and this one) are very close, and their difference is comparable or smaller than that caused by other selections. We compute standard errors for linear regression parameters using equation (4) of Stock and Smith (2000): $d = 3.07 \pm 0.24$, $d = 3.08 \pm 0.30$, $d = 2.84 \pm 0.37$, and $d = 3.16 \pm 0.70$, for all events, thrust events, normal events, and strike-slip events, respectively. These values differ only marginally from the standard case (see previous section), confirming our conclusion. As we mentioned previously, to estimate the scaling exponent for the Harvard data, we can ignore seismic moment errors.

Table 1 lists several other cases where the aftershock selection criteria are modified as explained in the Data Selection section. The values of regression parameters are similar to the standard case, the difference usually within a 1σ or 2σ level. The only exception is the distance window selection, $r = 500$ km, meaning that for all mainshocks, aftershocks are selected within a 500-km radius. Apparently, when we use a 500-km circle to select aftershocks, some other randomly occurring nonaftershock events are included.

A change in the minimum number of aftershocks (N_a) does not influence the regression parameter values. This is important because many of 231 $m \geq 7$ shallow mainshocks

lack sufficient aftershock sequences to infer their size. However, as mentioned previously, our estimation procedure is not biased. Thus, if catalogs with the magnitude threshold lower than that of the PDE were available, the results should not be substantially altered.

How do location errors influence the size of the aftershock ellipses? Only mutual distances between the aftershocks are significant in our measurements. Thus, relative random location errors affect the ellipse axes size. If location errors are statistically independent, the semiaxes increase as

$$\sigma_x^2 = \sigma_o^2 + \varepsilon^2, \tag{27}$$

where ε is the location error, σ_x is a major or minor semiaxis, and σ_o is its real value. Smith and Ekström (1997) suggested that the combined relative error in the centroid and hypocenter locations is on the order of 25 km. The relative error of earthquake location in the PDE catalog can be roughly estimated from the reported standard deviations of the origin time. These standard errors are on the order of 1 sec on average, so we take $\varepsilon = 7.5$ km to demonstrate how these errors affect the scaling exponent determination (see row 8 in Table 1). Again, the regression coefficient values are similar to the standard case. A comparison of matched shallow earthquakes in the PDE and ISC catalogs yields a standard deviation for the difference between the origin times of about 1.6–1.8 sec. If time accuracy is equal in both catalogs, this would imply that the origin time errors in the catalogs are slightly over 1 sec ($\sigma_t \approx 1.7/\sqrt{2}$). More details are available in the article by Kagan (2002).

Discussion

Our results suggest that seismic moment M depends on rupture length l as

$$M \propto l^3, \tag{28}$$

up to at least $l = 250$ km, that is, for the largest earthquake size registered by the Harvard catalog ($M \geq 10^{21}$ N m). This relation apparently does not depend on the type of earthquake focal mechanism. Given the small magnitude range of our measurements, the d exponent is determined with a large uncertainty, and a scaling break cannot be reliably investigated. However, we can rule out a significant scaling break simply because $d = 3$ for small and intermediate earthquakes (Abercrombie, 1995), and the exponent seems to have the same value for large ($m \approx 8$) events. The previously held opinion that very large earthquakes ($m \geq 7.5$) and especially strike-slip events have a smaller slope d has been based on old data that are subject to doubt.

Studies of earthquake size distribution (Kagan, 2002a) also suggest that distribution is the same for earthquakes of different focal mechanisms. This conclusion contradicts the hypothesis that for strike-slip earthquakes the magnitude–frequency relation should saturate earlier than the other events (Pacheco *et al.,* 1992). Houston (2001) found that for strike-slip earthquakes total rupture time is equal or even smaller than for those with other focal mechanisms. This finding also seems incompatible with the hypothesis that strike-slip rupture for large events is confined to a long, narrow brittle layer (Stock and Smith, 2000). If the previous conjecture is true, strike-slip earthquakes of equal size with thrust events should have a more extended rupture and hence a longer rupture time.

Pacheco *et al.* (1992) also suggested that subduction zone earthquakes have a break in the magnitude–frequency relation at about m 7.5 due to a changed scaling relation. This conjecture is not supported by recent studies of earthquake size distribution (Main, 2000; Kagan, 2002a,b; Leonard *et al.,* 2001). Figures 6 and 7 also lack any scaling break corresponding to m 7.5 events.

The largest event in 1977–2000 was the 19 August 1977 Sumba (Indonesia) earthquake, M 3.59 $\times$ 10^{21} N m. No really great earthquakes ($M \geq 10^{22}$ N m) occurred during this time (more discussion in Kagan, 2002a), so our conclusions may be considered tentative. Except for the unusual 1998 Antarctic earthquake, the largest aftershock zones do not exceed 300 km (see the Appendix). Much larger earthquake ruptures extending over several hundred km are known from instrumental catalogs of the early and middle twentieth century and from historical records (Wells and Coppersmith, 1994; Stock and Smith, 2000). Long ruptures of strike-slip earthquakes (for example, in California, extending over 400 km) are especially important here. Since strike-slip earthquakes are less common than thrust events, the historic and instrumental record for them is even spottier. However, their moment-frequency relation, as well as the value of the possible earthquake maximum size, seem similar to the latter events (Kagan, 2002a,b). This implies that truly great strike-slip earthquakes can occur.

If the reported scaling regularities are correct, what conclusions can be drawn from this? According to equations (1)–(3), as soon as the rupture width W exceeds the thickness of the brittle layer, $d = 3$ can be explained either by slip u increasing much faster than

$$u \propto M^{1/3}, \tag{29}$$

or the width continuing to enlarge as the earthquake size increases. The former case would imply that very large earthquakes should have a larger strain drop than do smaller events, a feature not reliably observed (cf. Toda and Stein, 2000). Hence $d = 3$ suggests that in large earthquakes, rupture penetrates into the lower crust and can be deeper. Although such a conclusion seems paradoxical, particularly for great earthquakes (see above), several studies support such a view.

For example, Anderson and Zhang (1991) analyzed the 23 May 1989 Macquarie ridge earthquake and concluded that a significant slip occurred below the Moho discontinuity during the earthquake. Abercrombie and Ekström (2001)

reached a similar conclusion for earthquakes on transform faults. Toda and Stein (2000) argued that the rupture depth for the Antarctic (Balleny Islands) earthquake of 25 March 1998 must have been at least 30 km. If extended to great earthquakes, scaling relations (28) and (29) would require a rupture width W of several tens of kilometers.

Rupture width is usually measured by a depth distribution of aftershocks. For strike-slip earthquakes occurring outside subduction zones, no aftershocks deeper than 20–25 km are observed, that is, where a significant slip during a mainshock seems required by the previous considerations. Apparently aftershocks are caused by stress heterogeneities induced by geometric and other complexities of rupture. Why then do we not observe aftershocks deeper than 20 km?

It is possible that if displacement occurs in the lower crust and upper mantle during and after great earthquakes, it may proceed at a slower rate not registered by standard seismographic equipment. There are indications that some tectonic deformation in the upper crust is released aseismically on the timescale of hours (Heki and Tamura, 1997; Takai *et al.,* 1999) or weeks and months (see, for example, Shen *et al.,* 1994; Heki *et al.,* 1997; McCaffrey, 1997; Ozawa *et al.,* 2001). Such a slip increases the total earthquake moment and may significantly increase the width W. Thus, scaling (28) would extend to great earthquakes if very low frequency were included.

It would be natural then (cf. Scholz, 1990, section 1.4) to assume that transition from a brittle to plastic deformation, that is, from earthquake rupture to plastic rock flow, is not sharp or discontinuous: a plastic slip in the lower crust and upper mantle would occur seemingly aseismically in the episodes of slow or ultraslow earthquakes with time constants on the order of minutes, hours, and days. Thus, the strain below the brittle upper crust may not occur as a steady-state flow but in relatively concentrated short-term episodes similar to earthquakes. For example, Dragert *et al.* (2001) (see also Thatcher, 2001) hypothesize that during the summer of 1999 an aseismic slip occurred in the Cascadia subduction zone as a discrete pulse equivalent to an earthquake with magnitude 6.7. These slow quasi earthquakes may not be observable by a seismographic network because their frequency range is largely below 1 mHz. Although this slow episodic deformation in the lower crust and upper mantle may not be seen easily by geodetic or GPS point observations because of its small amplitude at the Earth surface, synthetic aperture radar interferometry (InSAR) may detect such events with a spatially wide correlation technique.

Conclusions

We compare the aftershock zone size and moment magnitude of a mainshock to infer the spatial scaling exponent for earthquakes. The following conclusions can be drawn:

1. A major source of uncertainty in determining the scaling exponent is probably the natural, random scatter of aftershocks.
2. For large ($m \geq 7$, $M \geq 10^{19.5}$ N m) earthquakes, the value of the spatial scaling exponent is close to 3.0, that is, the same as for small and moderate events.
3. No observable saturation occurs in aftershock area size for large earthquakes ($M \geq 10^{21}$ N m).
4. The scaling exponent value does not depend on the earthquake focal mechanism: strike-slip earthquakes exhibit the same scaling behavior as thrust or normal events.

Acknowledgments

I appreciate partial support from the National Science Foundation through grant EAR 00-01128. I also appreciate support from the National Science Foundation through Cooperative Agreement EAR-8920136 and USGS Cooperative Agreement 14-08-0001-A0899 and 1434-HQ-97AG01718 to the Southern California Earthquake Center (SCEC). I thank D. D. Jackson, P. Bird, H. Houston (UCLA), I. Main (University of Edinburgh), and C. Stock (Victoria University) for very useful discussions and S. Das (Oxford University) for sending me G. Pegler's Ph.D. Thesis. I am grateful to C. Henry and S. Das who sent me their article before its publication. The comments by the reviewers Rachel Abercrombie and Ian Main as well as by the Associate Editor Cezar Trifu have greatly improved the presentation of the methods and the results. This is SCEC Publication No. 603.

References

Abercrombie, R. E. (1995). Earthquake source scaling relationships from -1 to 5 M_L using seismograms recorded at 2.5-km depth, *J. Geophys. Res.* **100,** 24,015–24,036.

Abercrombie, R. E., and G. Ekström (2001). Earthquake slip on oceanic transform faults, *Nature* **410,** 74–77.

Anderson, H. J., and J. J. Zhang (1991). Long-period seismic radiation from the May 23, 1989, Macquarie ridge earthquake: evidence for coseismic slip in the mantle, *J. Geophys. Res.* **96,** 19,853–19,863.

Antolik, M., A. Kaverina, and D. S. Dreger (2000). Compound rupture of the great 1998 Antarctic plate earthquake, *J. Geophys. Res.* **105,** 23,825–23,838.

Bodin, P., and J. N. Brune (1996). On the scaling of slip with rupture length for shallow strike-slip earthquakes: quasi-static models and dynamic rupture propagation, *Bull. Seism. Soc. Am.* **86,** 1292–1299.

Dragert, H., K. Wang, and T. S. James (2001). A silent slip event on the deeper Cascadia subduction interface, *Science* **292,** 1525–1528.

Dziewonski, A. M., G. Ekström, and N. N. Maternovskaya (2001). Centroid-moment tensor solutions for April-June 2000, *Phys. Earth Planet. Interiors* **123,** 1–14.

Frohlich, C. (2001). Display and quantitative assessment of distributions of earthquake focal mechanisms, *Geophys. J. Int.* **144,** 300–308.

Fujii, Y., and M. Matsu'ura (2000). Regional difference in scaling laws for large earthquakes and its tectonic implication, *Pure Appl. Geophys.* **157,** 2283–2302.

Geller, R. J. (1976). Scaling relations for earthquake source parameters and magnitudes, *Bull. Seism. Soc. Am.* **66,** 1501–1523.

Heki, K., and Y. Tamura (1997). Short term afterslip in the 1994 Sanriku-Haruka-Oki earthquake, *Geophys. Res. Lett.* **24,** 3285–3288.

Heki, K., S. Miyazaki, and H. Tsuji (1997). Silent fault slip following an interplate thrust earthquake at the Japan Trench, *Nature* **386,** 595–598.

Helffrich, G. R. (1997). How good are routinely determined focal mechanisms? Empirical statistics based on a comparison of Harvard, USGS and ERI moment tensors, *Geophys. J. Int.* **131,** 741–750.

Henry, C., and S. Das (2001). Aftershock zones of large shallow earthquakes: fault dimensions, aftershock area expansion, and scaling relations, *Geophys. J. Int.* **147,** 272–293.

Henry, C., S. Das, and J. H. Woodhouse (2000). The great March 25, 1998, Antarctic Plate earthquake: moment tensor and rupture history, *J. Geophys. Res.* **105,** 16,097–16,118.

Hill, D. P., P. A. Reasenberg, A. Michael, W. J. Arabaz, G. Beroza, D. Brumbaugh, J. N. Brune, R. Castro, S. Davis, D. DePolo, W. L. Ellsworth, J. Gomberg, S. Harmsen, L. House, S. M. Jackson, M. J. S. Johnston, L. Jones, R. Keller, S. Malone, L. Munguia, S. Nava, J. C. Pechmann, A. Sanford, R. W. Simpson, R. B. Smith, M. Stark, M. Stickney, A. Vidal, S. Walter, V. Wong, and J. Zollweg (1993). Seismicity remotely triggered by the magnitude 7.3 Landers, California, earthquake, *Science* **260,** 1617–1623.

Houston, H. (2001). Influence of depth, focal mechanism, and tectonic setting on the shape and duration of earthquake source time functions, *J. Geophys. Res.* **106,** 11,137–11,150.

Kagan, Y. Y. (1991). Likelihood analysis of earthquake catalogues, *Geophys. J. Int.* **106,** 135–148.

Kagan, Y. Y., and D. D. Jackson (1999). Worldwide doublets of large shallow earthquakes, *Bull. Seism. Soc. Am.* **89,** 1147–1155.

Kagan, Y. Y. (2002a). Seismic moment distribution revisited. I. Statistical results, *Geophys. J. Int.* (in press); available at *http://scec.ess.ucla.edu/~ykagan/moms_index.html* (last accessed February 2002).

Kagan, Y. Y. (2002b). Seismic moment distribution revisited. II. Moment conservation principle, *Geophys. J. Int.* (in press); *http://scec.ess.ucla.edu/~ykagan/momc_index.html* (last accessed February 2002).

Kagan, Y. Y. (2002c). Accuracy of modern global earthquake catalogs, *Phys. Earth Planet Interiors* (submitted), *http://scec.ess.ucla.edu/~ykagan/scal_index.html* (last accessed February 2002).

Kagan, Y. Y., and D. D. Jackson (2002?). Probabilistic forecasting of earthquakes, *Geophys. J. Int.,* **143,** 438–453.

Kanamori, H., and D. Anderson (1975). Theoretical basis of some empirical relations in seismology, *Bull. Seism. Soc. Am.* **65,** 1073–1095.

Leonard, T., O. Papsouliotis, and I. G. Main (2001). A Poisson model for identifying characteristic size effects in frequency data: application to frequency-size distributions for global earthquakes, "starquakes" and fault lengths, *J. Geophys. Res.* **106,** 13,473–13,484.

Mai, P. M., and G. C. Beroza (2000). Source scaling properties from finite-fault-rupture models, *Bull. Seism. Soc. Am.* **90,** 604–615.

Main, I. (2000). Apparent breaks in scaling in the earthquake cumulative frequency-magnitude distribution: fact or artifact? *Bull. Seism. Soc. Am.* **90,** 86–97.

McCaffrey, R. (1997). Influence of recurrence times and fault zone temperatures on the age-rate dependence of subduction zone seismicity, *J. Geophys. Res.* **102,** 22,839–22,854.

McGuire, J. J., Li Zhao, and T. H. Jordan (2000). Rupture dimensions of the 1998 Antarctic earthquake from low-frequency waves, *Geophys. Res. Lett.* **27,** 2305–2308.

Ogata, Y. (1998). Space-time point-process models for earthquake occurrences, *Ann. Inst. Statist. Mech.* **50**, no. 2, 379–402.

Ozawa, S., M. Murakami, and T. Tada (2001). Time-dependent inversion study of the slow thrust event in the Nankai trough subduction zone, southwestern Japan, *J. Geophys. Res.* **106,** 787–802.

Pacheco, J. F., C. H. Scholz, and L. R. Sykes (1992). Changes in frequency-size relationship from small to large earthquakes, *Nature* **355,** 71–73.

Pegler, G. (1995). Studies in seismotectonics, *Ph. D. Thesis,* University of Oxford, U.K., pp. 234.

Pegler, G., and S. Das (1996). Analysis of the relationship between seismic moment and fault length for large crustal strike-slip earthquakes between 1977–92, *Geophys. Res. Lett.* **23,** 905–908.

Preliminary Determination of Epicenters (PDE) (2000) Monthly Listings, U.S. Dept. Interior/Geol. Survey, Nat. Earthquake Inform. Center (NEIC), November, 32 pp. See also *http://neic.usgs.gov/neis/epic/epic.html* (last accessed February 2002).

Press, W. H., S. A. Teukolsky, W. T. Vetterling, and B. P. Flannery (1992). *Numerical Recipes in FORTRAN,* Second Ed., Cambridge University Press, New York, pp. 963.

Romanowicz, B. (1994). A reappraisal of large earthquake scaling: comment, *Bull. Seism. Soc. Am.* **84,** 1675–1676.

Sato, R. (1979). Theoretical basis on relationships between focal parameters and earthquake magnitude, *J. Phys. Earth* **27,** 353–372.

Scholz, C. H. (1990). *The Mechanics of Earthquakes and Faulting,* Cambridge University Press, New York, pp. 439.

Scholz, C. H. (1997). Size distributions for large and small earthquakes, *Bull. Seism. Soc. Am.* **87,** 1074–1077.

Scholz, C. H. (1998). A further note on earthquake size distributions, *Bull. Seism. Soc. Am.* **88,** 1325–1326.

Shaw, B. E., and C. H. Scholz (2001). Slip-length scaling in large earthquakes: Observations and theory and implications for earthquake physics, *Geophys. Res. Lett.* **15,** 2995–2998.

Shen, Z.-K., D. D. Jackson, Y. J. Feng, M. Cline, M. Kim, P. Fang, and Y. Bock (1994). Postseismic deformation following the Landers earthquake, California, 28 June 1992, *Bull. Seism. Soc. Am.* **84,** 780–791.

Sipkin, S. A., C. G. Bufe, and M. D. Zirbes (2000). Moment-tensor solutions estimated using optimal filter theory: global seismicity, 1999, *Phys. Earth Planet. Interiors* **122,** 147–159.

Smith, G. P., and G. Ekström (1997). Interpretation of earthquake epicenter and CMT centroid locations, in terms of rupture length and direction, *Phys. Earth Planet. Interiors* **102,** 123–132.

Stock, C., and E. G. C. Smith (2000). Evidence for different scaling of earthquake source parameters for large earthquakes depending on faulting mechanism, *Geophys. J. Int.* **143,** 157–162.

Takai, K., H. Kumagai, and N. Fujii (1999). Evidence for slow slip following a moderate-size earthquake (M_w = 5.7) in a subducting plate, *Geophys. Res. Lett.* **26,** 2113–2116.

Thatcher, W. (2001). Silent slip on the Cascadia subduction interface, *Science* **292,** 1495–1496.

Toda, S., and R. S. Stein (2000). Did stress triggering cause the large off-fault aftershocks of the 25 March 1998 M_w = 8.1 Antarctic plate earthquake? *Geophys. Res. Lett.* **27,** 2301–2304.

Utsu, T. (1969). Aftershocks and earthquake statistics. I. Some parameters which characterize an aftershock sequence and their interrelations, *J. Fac. Sci. Hokkaido Univ. Jpn Ser. VII* **3,** 129–195.

Wang, J. H., and S. S. Ou (1998). On scaling of earthquake faults, *Bull. Seism. Soc. Am.* **88,** 758–766.

Wells, D. L., and K. J. Coppersmith (1994). New empirical relationships among magnitude, rupture length, rupture width, rupture area, and surface displacement, *Bull. Seism. Soc. Am.* **84,** 974–1002.

York, D. (1966). Least-squares fitting of a straight line, *Can. J. Phys.* **44,** 1079–1086.

York, D. (1967). The best isochron, *Earth Planet. Sci. Lett.* **2,** 479–482.

Department of Earth and Space Sciences
University of California
Los Angeles, California 90095-1567

Manuscript received 21 May 2001.

Appendix

Mainshock									Aftershocks						*T*-axis		*P*-axis	
No.	W_a*	Year	Month	Day	*H*	*M*	Latitude	Longitude	m_w	N_a†	Latitude	Longitude	4σ‡	Focal Mech.§	Pl.	Az.	Pl.	Az.
1	1	1977	3	18	21	44	16.38	122.59	7.30	21	16.76	122.45	91.989	Thr	69	259	19	103
5	2	1977	4	21	4	24	−10.22	160.59	7.39	25	−10.09	160.55	144.555	Thr	78	96	10	244
8	3	1977	8	19	6	9	−11.14	118.23	8.37	27	−10.96	118.82	286.549	Nor	21	157	67	317
13	4	1977	11	23	9	26	−31.22	292.31	7.51	30	−31.38	292.38	87.214	Thr	89	289	1	94
15	5	1978	3	23	0	31	43.81	149.23	7.10	43	44.18	149.22	93.739	Thr	65	303	25	130
16	6	1978	3	23	3	15	44.12	149.27	7.62	45	44.25	149.40	105.416	Thr	56	312	34	132
17	7	1978	3	24	19	48	44.20	148.98	7.57	58	44.07	148.82	105.844	Thr	63	309	27	131
24	8	1978	11	4	22	29	−11.16	161.82	7.04	10	−11.19	162.23	44.006	Thr	53	106	22	229
37	9	1979	12	12	8	0	2.32	281.19	8.15	15	2.54	280.96	282.369	Thr	58	81	31	278
41	10	1980	7	8	23	19	−12.92	166.21	7.53	14	−12.65	166.03	126.730	Thr	81	320	4	75
42	11	1980	7	17	19	43	−12.44	165.94	7.79	11	−12.14	166.09	222.253	Thr	74	49	14	253
43	12	1980	10	10	12	25	36.25	1.36	7.14	10	36.21	1.53	76.084	Thr	73	298	15	146
45	13	1980	10	25	7	0	−22.16	169.83	7.15	10	−22.03	169.89	150.529	Thr	69	16	19	221
46	14	1980	10	25	11	0	−21.76	169.84	7.51	18	−21.99	169.76	149.894	Thr	67	36	23	230
52	15	1981	7	15	7	59	−17.34	167.27	7.17	22	−17.35	167.59	136.442	Thr	72	84	18	253
54	16	1981	9	1	9	29	−15.02	186.84	7.53	12	−15.28	186.92	144.049	Nor	9	12	76	143
67	17	1982	12	19	17	44	−24.31	184.90	7.53	24	−24.21	184.28	166.943	Thr	66	269	23	100
70	18	1983	5	26	3	0	40.44	138.87	7.77	42	40.76	139.12	175.560	Thr	72	114	18	289
74	19	1983	11	30	17	46	−6.35	71.75	7.74	29	−6.73	71.78	184.495	Nor	15	176	64	299
77	20	1984	3	19	20	28	40.59	63.24	7.03	13	40.30	63.29	60.525	Thr	66	314	24	130
81	21	1985	3	3	22	47	−33.92	288.29	8.01	38	−33.50	288.10	217.109	Thr	68	61	20	266
82	22	1985	3	4	0	32	−33.06	288.21	7.41	22	−33.26	288.10	134.793	Thr	49	223	26	99
84	23	1985	5	10	15	36	−5.68	150.97	7.23	12	−5.63	151.06	89.294	Ss	7	147	25	53
85	24	1985	7	3	4	37	−4.28	152.58	7.28	16	−4.43	152.77	81.536	Thr	77	200	9	68
86	25	1985	8	23	12	42	39.54	750.09	7.01	17	39.53	75.25	85.757	Thr	48	304	30	175
90	26	1985	11	28	3	50	−13.76	166.08	7.04	14	−13.94	166.25	49.423	Ss	24	123	7	216
92	27	1986	5	7	22	47	51.33	184.57	8.01	94	51.39	184.63	230.693	Thr	67	346	23	160
93	28	1986	8	14	19	39	2.08	126.89	7.57	22	2.01	126.79	120.849	Thr	52	150	35	302
94	29	1986	10	20	6	46	−27.93	183.93	7.77	48	−27.83	183.64	165.778	Ss	38	236	10	138
95	30	1986	11	14	21	20	23.97	121.85	7.41	15	23.92	121.93	81.561	Thr	77	308	12	122
97	31	1987	2	8	18	34	−5.90	147.72	7.37	20	−5.98	147.74	110.503	Ss	8	307	3	37
102	32	1987	10	12	13	57	−7.12	154.05	7.02	12	−7.17	154.32	63.347	Nor	5	217	74	324
112	33	1988	8	10	4	38	−10.49	160.77	7.60	20	−10.30	160.74	128.531	Thr	61	35	28	235
114	34	1988	11	6	13	3	23.00	99.68	7.04	10	23.13	99.55	142.462	Ss	13	289	4	198
115	35	1989	2	10	11	15	2.64	126.72	7.16	33	2.36	126.64	43.277	Thr	76	126	14	299
118	36	1989	11	1	18	25	39.95	143.08	7.42	17	39.65	143.24	138.764	Thr	57	302	32	111
119	37	1989	12	15	18	44	7.88	126.96	7.58	37	8.05	126.79	146.746	Thr	71	330	13	103
120	38	1990	3	3	12	16	−22.05	175.35	7.65	13	−21.78	175.27	275.201	Ss	18	90	13	184
123	39	1990	4	5	21	12	15.57	148.08	7.47	45	15.40	147.60	104.479	Nor	15	108	72	320
124	40	1990	4	18	13	39	1.31	123.35	7.68	37	1.24	123.20	126.070	Thr	66	135	17	0
128	41	1990	6	20	21	0	36.95	49.52	7.42	18	37.05	49.53	177.248	Ss	34	163	9	67
129	42	1990	7	16	7	26	15.97	121.23	7.74	70	16.14	120.75	200.650	Ss	4	198	2	108
131	43	1991	4	22	21	57	10.10	277.23	7.68	14	9.75	276.82	145.683	Thr	63	249	23	37
132	44	1991	4	29	9	12	42.60	43.61	7.01	22	42.54	43.77	90.400	Thr	77	311	7	186
137	45	1991	12	22	8	43	45.58	151.55	7.63	25	45.18	151.80	146.911	Thr	61	303	29	129

141	46	1992	5	17	9	49	7.27	126.96	7.13	18	7.19	127.04	125.304	Thr	63	334	20	110
142	47	1992	5	17	10	15	7.33	127.18	7.28	18	7.23	127.05	146.653	Thr	66	308	22	103
144	48	1992	6	28	11	57	34.65	243.35	7.35	11	34.30	243.28	158.034	Ss	9	296	20	202
145	49	1992	8	19	2	4	42.19	73.32	7.26	14	42.03	73.44	71.063	Thr	73	21	14	171
146	50	1992	9	2	0	16	11.20	272.19	7.69	40	11.50	272.61	272.132	Thr	57	32	33	212
147	51	1992	10	18	15	12	7.27	283.66	7.17	26	7.20	283.43	136.422	Ss	38	241	23	132
148	52	1992	12	12	5	29	−8.34	122.49	7.80	29	−8.50	122.31	172.885	Thr	84	130	5	346
150	53	1993	3	6	3	6	−10.73	164.02	7.15	13	−10.99	164.08	119.884	Ss	28	109	19	210
153	54	1993	7	12	13	17	42.71	139.28	7.78	40	42.61	139.24	184.221	Thr	80	88	10	270
154	55	1993	8	8	8	34	13.06	145.31	7.81	15	13.10	145.12	191.224	Thr	52	327	34	177
156	56	1993	9	10	19	13	14.41	267.01	7.28	15	14.21	267.04	90.747	Thr	68	45	21	209
162	57	1994	6	2	18	18	−11.03	113.04	7.82	20	−10.86	112.73	306.953	Thr	52	9	38	189
163	58	1994	7	13	2	36	−16.50	167.35	7.21	24	−16.71	167.35	109.744	Ss	33	125	31	238
165	59	1994	10	4	13	23	43.60	147.63	8.32	147	43.65	147.46	242.713	Thr	46	359	20	112
166	60	1994	10	9	7	55	43.87	147.96	7.31	20	43.63	147.87	113.440	Thr	63	294	27	125
168	61	1994	12	28	12	19	40.56	142.99	7.79	28	40.18	143.33	156.246	Thr	56	298	34	108
170	62	1995	2	5	22	51	−37.61	179.40	7.18	14	−37.80	178.84	59.098	Nor	13	305	77	124
171	63	1995	4	21	0	34	12.27	125.69	7.21	61	12.06	125.66	93.265	Thr	63	291	25	85
172	64	1995	5	5	3	53	12.67	125.30	7.11	18	12.56	125.29	84.624	Thr	59	270	30	75
173	65	1995	5	16	20	13	−23.05	170.00	7.73	48	−23.02	170.25	138.580	Nor	11	196	78	42
176	66	1995	7	30	5	11	−24.17	289.26	8.05	53	−24.00	289.48	229.770	Thr	67	90	23	267
177	67	1995	8	16	10	28	−5.51	153.64	7.77	29	−5.57	153.84	202.857	Thr	86	259	3	48
178	68	1995	8	16	23	10	−6.08	154.19	7.23	19	−6.02	154.13	139.112	Thr	89	157	0	42
180	69	1995	10	3	1	51	−2.55	282.47	7.06	18	−2.72	282.23	76.250	Thr	69	241	10	123
182	70	1995	10	18	10	37	28.06	130.18	7.17	32	28.06	130.19	80.774	Nor	19	292	66	148
184	71	1995	12	3	18	1	44.82	150.17	7.95	91	44.66	149.96	171.754	Thr	57	309	33	131
187	72	1996	2	17	6	0	−0.67	136.62	8.25	86	−0.86	136.38	257.386	Thr	55	220	35	31
189	73	1996	2	25	3	8	15.88	262.02	7.16	15	16.03	262.17	67.209	Thr	61	33	29	203
191	74	1996	6	10	4	4	51.10	182.59	7.94	55	51.28	182.74	173.582	Thr	61	347	29	163
192	75	1996	6	10	15	25	51.38	183.51	7.29	18	51.31	183.50	101.756	Thr	68	318	21	157
195	76	1996	11	12	17	0	−15.04	284.63	7.77	25	−15.19	284.52	125.694	Thr	65	117	16	247
197	77	1997	2	27	21	8	29.74	68.13	7.15	13	29.72	68.26	100.926	Thr	57	344	31	182
198	78	1997	4	21	12	3	−13.21	166.20	7.76	42	−13.32	166.36	123.190	Thr	57	131	15	245
199	79	1997	5	10	7	57	33.58	60.02	7.25	10	33.24	60.12	122.559	Ss	5	113	5	203
204	80	1997	12	5	11	27	54.31	161.91	7.82	139	54.17	161.84	184.349	Thr	66	321	23	124
206	81	1998	3	25	3	13	−62.99	148.64	8.15	14	−62.99	147.14	460.547	Ss	16	146	7	54
209	82	1998	7	17	8	49	−2.50	142.07	7.04	10	−2.85	142.22	53.250	Thr	59	181	29	26
212	83	1998	11	29	14	10	−2.03	125.00	7.77	10	−1.90	124.55	135.993	Ss	1	324	38	55
215	84	1999	8	17	0	1	41.01	29.97	7.64	15	40.69	30.42	181.426	Ss	13	45	10	138
216	85	1999	9	20	17	47	24.15	120.80	7.69	36	23.77	121.12	97.136	Thr	70	116	20	303
222	86	1999	11	26	13	21	−16.08	168.31	7.48	15	−15.96	168.03	94.583	Thr	70	317	17	100
226	87	2000	5	4	4	21	−1.29	123.59	7.59	19	−1.30	123.47	99.491	Ss	23	185	13	89
227	88	2000	6	4	16	28	−4.73	101.94	7.91	64	−4.96	102.35	217.980	Ss	42	60	7	323
229	89	2000	11	16	4	55	−4.56	152.79	8.06	124	−5.08	153.08	217.769	Ss	33	181	29	292
230	90	2000	11	16	7	42	−5.03	153.17	7.87	112	−5.14	153.06	249.297	Thr	60	339	30	160
231	91	2000	11	17	21	2	−5.26	152.34	7.83	71	−5.23	152.74	254.902	Thr	65	7	22	160

*Number of mainshocks with 10 or more aftershocks.

†Number of aftershocks.

‡Two times major axis of aftershock ellipse, 2σ confidence area length.

§Ss, strike slip; Thr, thrust; Nor, normal.